PROGRESS IN THE DEVELOPMENT OF A TIME-TO-CONTACT AUTOROTATION CUEING SYSTEM

Michael Jump*, Mushfiqul Alam*, Jonathan Rogers**, Brian Eberle**
*The University of Liverpool, Liverpool, United Kingdom
**Georgia Institute of Technology, Atlanta, Georgia, United States

Abstract
Autorotation to landing is a difficult manoeuvre to accomplish successfully in an emergency. During autorotation, it is critical to simultaneously maintain the desired flight path, decelerate the aircraft appropriately, all whilst locating and reaching a safe location to land. This significantly increases the pilot work load in the cockpit. Therefore, there is a clear need to develop a set of pilot cueing and control augmentation technologies that lead to a higher probability of a successful autorotation landing. Tau theory and the associated guides have been shown be of benefit when used to provide guidance cueing in flight, where 'tau' is the instantaneous time-to-contact a surface at the current rate of closure. This article presents a detailed analysis of real autorotation flight data in the tau domain. The findings indicate that the taus of pitch angle and range distance can be modelled as being coupled to intrinsic tau motion guides (constant acceleration and deceleration respectively). Additionally, the article presents the development and analysis of a method to generate deceleration trajectories in autorotation using tau as the basis. A point mass model is used to rapidly evaluate trajectory feasibility and enforce reachability constraints in an autorotative flare. This approach of using a low-order model to evaluate reachability shows promise in terms of both accuracy and runtime guarantees. The tau-based control and tau-based trajectory generation schemes can be combined to create a control augmentation system in which reachable areas are depicted visually to the pilot, and inceptor cues are given to reach a selected desired landing point.

Nomenclature

C_P	Power coefficient
C_T	Thrust coefficient
C_x	Horizontal component of thrust
C_z	Vertical component of thrust
c_{d0}	Mean profile-drag coefficient of rotor blades
I_R	Main rotor moment of inertia
P_s	Residual shaft power
V_{grnd}	Velocity over ground
Z_{dot}	Vertical velocity
R	Main rotor radius
g	Gravitational constant
h	Altitude above touchdown point
q	Pitch rate
m	Vehicle total mass
u	Forward velocity
w	Vertical velocity
x	Longitudinal distance
f_e	Fuselage equivalent flat plate drag area
α	Main rotor tip path plane angle
η	Main rotor efficiency factor
λ	Main rotor inflow ratio
ρ	Air density
σ	Main rotor solidity
Ω	Main rotor angular velocity
θ	Pitch angle
θ_0	Main rotor collective blade pitch
θ_{1s}	Main rotor longitudinal cyclic pitch
τ	Time-to-contact
τ_p	Turboshaft engine power time constant
$\tau_{g_{CDG}}$	Constant deceleration intrinsic guide
$\tau_{g_{CAG}}$	Constant acceleration intrinsic guide

1. INTRODUCTION

Autorotation to land is a complex flight manoeuvre requiring several piloting tasks to be coordinated simultaneously to ensure a successful outcome. There is a need to develop autorotation control laws to serve as pilot assistance devices to allow the pilot to focus on other important tasks which are difficult to automate, such as selecting a suitable landing site. Therefore, it is considered to be highly desirable to provide the pilot with guidance during the autorotation manoeuvre to alleviate high pilot work load and to mitigate against the potentially catastrophic consequences of mistiming the manoeuvre. Likewise, for fully-autonomous rotorcraft, an automated autorotation landing system is likely to be required for certification to minimize risk to those not involved in the flight.

Previous pilot cueing work reported by the authors

Presented at 44th European Rotorcraft Forum, Delft, The Netherlands, 19-20 September, 2018

focused on developing a head-up display (HUD) to aid the pilot with the timing and magnitude of longitudinal cyclic and collective inputs during the autorotation manoeuvre[1]. This HUD was driven by an autorotation control law developed previously by the authors that can safely control the vehicle through the autorotation manoeuvre[2]. Rogers et al[3] describes a system by which the capability to land at a desired touchdown position can be incorporated into the control law put forward by Sunberg et al[2]. This trajectory-generating algorithm outputs a forward speed deceleration profile that can be tracked during the flare phase of the autorotation manoeuvre to ensure landing within a reasonable distance of the desired touchdown position.

Initial prior work by Lee et al[4] used an optimal control approach to show that the height-velocity avoid region can be reduced significantly using automated autorotation control. Abbeel et al[5] and Dalamagkis et al[6] studied machine learning strategies for this purpose. The former demonstrated successful autorotation of a model helicopter. Yomchinda et al[7] and Tierney and Langelaan[8] developed autorotation path planning and flare control laws, where the flare controller was derived through a direct optimal control approach. Several others, including Keller et al[9] and Bachelder et al[10], have developed pilot-in-the-loop autorotation control augmentation systems. Boeing's Helicopter Active Control Technology Program addressed the problem of tactile feedback during steady-state autorotative descent using a neural network[11].

The most difficult aspect of autorotation to automate (besides selection of a landing site) is the generation of a feasible flare trajectory[8]. Typically[4,7,8,10] the control inputs are discretised in time over the flare trajectory and optimized iteratively. This poses problems for certification due to convergence guarantees (if implemented online) or the ability to handle all possible landing scenarios (if implemented offline using a trajectory database). To try to solve these problems, the authors have developed a piecewise expert system controller that exhibits deterministic runtime and guaranteed convergence[2]. A key aspect here is that the vehicle descent rate is controlled to match a desired time-to-ground-contact. Feasible flare trajectories from a broad range of entry conditions can thus be determined. The use of time-to-contact (tau) in the closed-loop dynamics creates a bridge with prior work on time-to-contact-based flight guidance strategies by Jump et al[12] for fixed-wing flare manoeuvres. Using the previous controller as a starting point, recent efforts have focused on 1) formalizing and improving tau-based autorotation guidance strategies and 2) investigating time-to-contact driven pilot cueing controller methodologies. An initial exploration of the latter objective was reported in Rogers et al[1].

2. TAU ANALYSIS

2.1. Preliminaries on Tau Theory and the Tau-Guide

Optical tau theory has been extensively investigated in recent research activities[13–15]. It is based on the fundamental parameter τ, which is the time-to-contact variable, originally posited in the optical field. The proposition is founded on the principle that purposeful actions are accomplished by coupling the motion under the control of an observer with either externally or internally generated guidance sources: the so-called motion guides[13,16].

The motivation for this line of investigation is that, in terms of visual guidance, the overall pilot's strategy is to overlay or close the gap between the perceived optical flow field and the required flight trajectory. The pilot then works directly with the available optical variables to achieve prospective control of the aircraft's future trajectory. Time to contact, τ, is defined by Eq. (1):

$$\tau(t) = \frac{x(t)}{\dot{x}(t)} \tag{1}$$

Here x is the motion gap to be closed, and $\dot{x}$ is the instantaneous gap closure rate. The term "motion gap" refers to a perceived difference between the observer's current and desired target states as shown in Fig. 1.

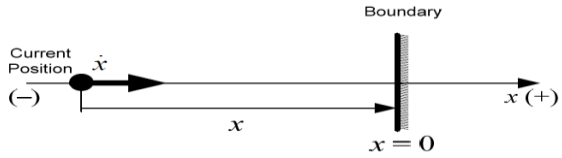

Fig. 1 Kinematics of closing a perceived motion gap.

Tau guidance of the observer's motion is achieved by using τ coupling: that is, keeping the tau of one optically available parameter in proportion with the tau of another. Such motion is then regulated by the coupling term, k (Eq. (2)). This coupling parameter plays a vital role in τ-theory, because it defines the kinematics of the motion.

In practice, there is often more than a single gap that needs to be closed, such as the coordination required between the lateral and longitudinal motions when an animal closes on its prey or forward and vertical motion required to land an aircraft[13]. The two motions, $x(t)$ and $y(t)$, are said

Presented at 44th European Rotorcraft Forum, Delft, The Netherlands, 19-20 September, 2018

to be τ coupled if the following relationship is satisfied:

$$\tau_x = k\tau_y \quad (2)$$

The constant coupling term, k in Eq. (2) regulates the dynamics of the motions in the x-direction and y-direction. By keeping the τ of motion gaps in constant ratio, it can be shown that this τ coupling results in effective guidance through a power law (for $x < 0$ and $y < 0$)[13].

$$y = C(-x)^{\frac{1}{k}} \quad (3)$$

The negative sign in Eq. (3) is due to the convention in τ theory that defines motion gaps as closing from negative to zero. Therefore the constant C must also be negative in order for y to be negative.

Tau coupling can take two forms: ***extrinsic*** (x and y are physically observable) or ***intrinsic*** (x is physically observable whereas y is generated by the actor's central nervous system). The second situation occurs when movements are self-guided and there is no second extrinsic motion gap to couple onto, for example when playing a piano. In this case, there is a physical gap to close (between finger and key), but the gap closure must be coupled to the rhythm of the tune being played, which is internally generated[13]. Under such a circumstance, the motion gap is hypothesized to be coupled onto a so-called ***intrinsic motion guide***. The intrinsic τ guide is modelled using the relationship:

$$\tau_x = k\tau_g \quad (4)$$

The intrinsic tau guide, τ_g defines a motion that is guiding a moving target with its own τ. It can take a number of different forms, but the most interesting and relevant for this paper are the constant acceleration guide (CAG) and constant deceleration guide (CDG). Examples of motion that can be generated by varying the values of the coupling constant k are shown in Fig. 2 and Fig. 3. For the detailed derivation of τ_g, see Lee and Padfield et al[14,16]. It can be observed that τ-coupled motion is only dependent upon parameters k and total time of the manoeuvre, T. The dressing "$\hat{}$" indicates that the temporal variables are normalized by T, which is the duration of the manoeuvre, such that $0 < \hat{t} \leq 1$. Detailed interpretation of the k values can be found in Appendix A.

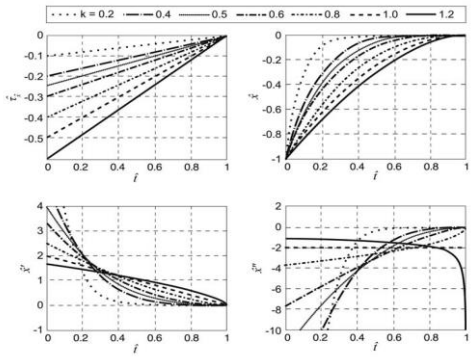

Fig. 2 Motion τ, gap distance, closure rate and acceleration when following a constant deceleration guide such that $\tau_x = k\tau_g$.

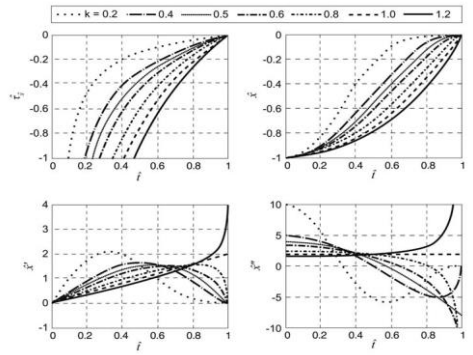

Fig. 3 Motion τ, gap distance, closure rate and acceleration when following a constant acceleration guide such that $\tau_x = k\tau_g$.

These remarkably simple equations form the guides that have been explored extensively in flight control research[14]. A key benefit of using τ-guided motion control is that it acts as a natural inverter of the system dynamics[18]. This can be achieved without necessarily needing to know the system model. In their earlier work, Rogers and Jump et al[3] presented an automatic autorotation controller (AAC) based on an analysis that focused on the tau of height above ground and tau of longitudinal distance to touchdown. The development of that AAC was based on the simulated autorotation test data performed using the HELIFLIGHT-R Simulator at the University of Liverpool. However, inspired in part by the ecological intrinsic motion guide findings of a pigeon's landing while trying to close the range distance gap[13,16,17], in this paper the analysis of gap closing during autorotation is extended to pitch angle and the range distance using τ-theory (discussed in Section 2.3).

2.2. Identification of the pilot strategy

In order to assess whether or not there is an identifiable autorotation strategy in the τ domain, a series of flight test autorotation manoeuvres, performed using the Bell 206 and Bell OH-58 Kiowa type helicopters, were analysed. The autorotation manoeuvre can be broken down into three phases from engine failure[3,19]: steady state

Presented at 44th European Rotorcraft Forum, Delft, The Netherlands, 19-20 September, 2018

descent, flare and touchdown. It has been shown by the work of Rogers and Jump et al.[3] that, in the steady state descent phase, as the name suggests, the rate of change of height and longitudinal distance remains reasonably constant, hence there are no significant motion gaps to close. During the autorotation to land manoeuvre, the flare phase is the most critical and most dynamic. The pilot must decelerate in both the vertical and horizontal axes correctly in close proximity to the ground and then achieve the correct landing attitude for touchdown. Hence, the analysis presented here focuses on the flare phase of the flight. The final 100ft of the longitudinal states in the flight test autorotations are shown in Fig. 4.

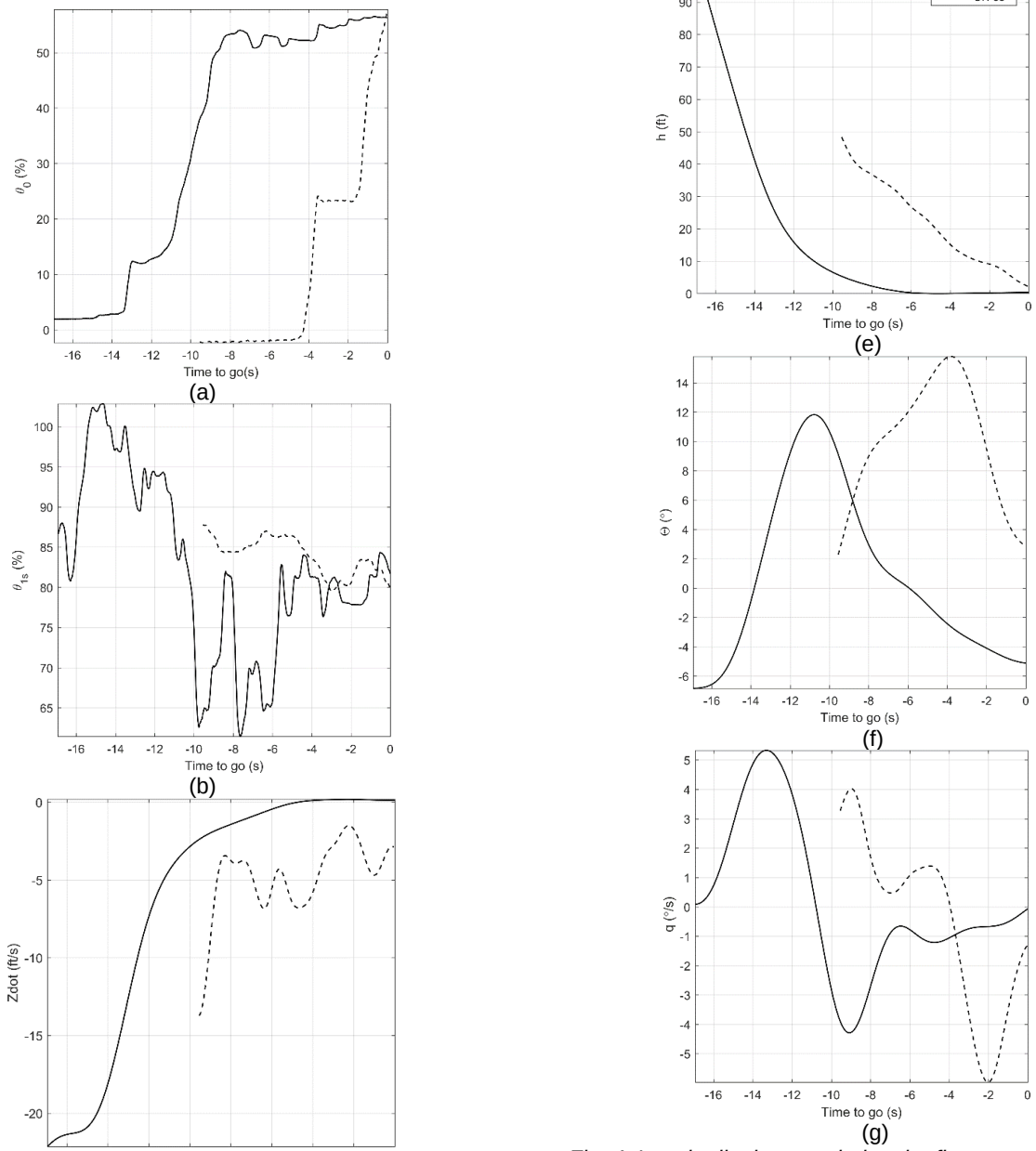

Fig. 4. Longitudinal states during the flare manoeuvre of autorotation using Bell OH-58 (solid lines) and Bell 206 type helicopter (dashed lines).

Presented at 44th European Rotorcraft Forum, Delft, The Netherlands, 19-20 September, 2018

Fig. 4 shows the result of what the authors consider to be "textbook" autorotation manoeuvres performed in the Bell 206 and OH-58 type helicopters. During the autorotation process, the pilot lowers the collective, see Fig. 4(a), and adjusts the helicopter's attitude using the longitudinal cyclic, see Fig. 4(b). This reduces the descent rate ($Zdot$), Fig. 4(c) and produces a constant desired forward speed (V_{grnd}), Fig. 4(d). At an altitude of approximately 50ft-100ft above the ground, see Fig. 4(e), the pilot initiates the flare by pulling back on the longitudinal cyclic. This pitches the helicopter's nose up to between 10-15 degrees from the initial pitch attitude, see Fig. 4(f). When the helicopter has reached the maximum pitch angle, the rotor speed increases, as does the descent rate. The pilot then applies a notional 'step' input to the collective to prevent the rotor speed rise and to reduce the descent speed. This condition is held for a short period of time (approximately 2-4 seconds) to allow the descent rate and forward speed to reduce. The pilot then levels the aircraft's pitch attitude (at an altitude of approximately 10-20ft). When the pitch attitude has been significantly reduced (to some small angle, Fig. 4(f)) the pilot applies more collective to further reduce the descent rate to below 10ft/s cushioning the landing during touchdown.

2.3. Analysis of the flight test data in Tau Domain for pitch angle and range distance

Tau theory is based upon the closure of so-called 'motion gaps'. In the flare phase of the autorotation manoeuvre, the most important goal is to reach the landing spot (closing height and longitudinal gap) and to perform a "soft" landing (reducing the touchdown speed – see Rogers and Jump et al.[3] for the limits of touchdown speed used in this study). The previous study provided cueing to the pilot by considering the motions in the different axes (height and longitudinal distance) independently. However, multitasking in movement guidance is made easier when the motions are synchronised, or can be orchestrated to be so. This study therefore focused on the extension of the tau analysis from previous work to two other motion gap closures considered to be important during the autorotation manoeuvre, as shown in Fig. 5, specifically:

I. The pitch angle, θ – to reduce forward speed and descent rate.
II. The range distance between the instantaneous position and landing spot (termed as $\boldsymbol{hx}$)

The distance to close the gap during flare is termed as hx and calculated as below:

(5) $$hx = \sqrt{h^2 + x^2}$$

Here h is the altitude above the target touchdown position and x is the longitudinal distance. The velocity for the corresponding range distance is found as:

(6) $$\dot{hx} = \frac{h\dot{h} + x\dot{x}}{\sqrt{h^2 + x^2}}$$

The tau of τ_{hx} can therefore be written as:

(7) $$\tau_{hx} = \frac{hx}{\dot{hx}} = \frac{h^2 + x^2}{h\dot{h} + x\dot{x}}$$

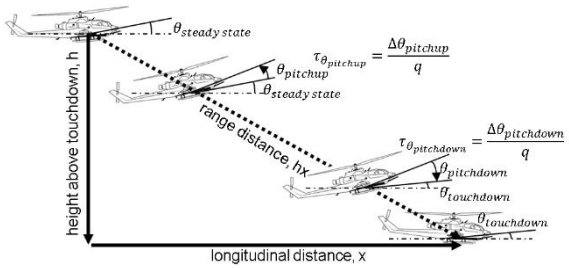

Fig. 5. Flare sequence during autorotative manoeuvre.

2.4. Tau analysis of Piloting Strategy using the gap closure of pitch angle and range distance

Range distance gap close, τ_{hx}

For the flight test data available, the tau of range distance was calculated using Eq. (7) and the results are plotted in Fig. 6. It can be seen that the trend in τ_{hx} closely resembles the features of intrinsic constant deceleration guide (CDG), $\tau_{g_{CDG}}$, profile as shown in Fig. 2. In order to see a clear trend in the parameters, the time of the flare phase of the autorotation manoeuvre has been normalized. Zero in the x axis indicates the start of the flare and 1 indicates the end of flare.

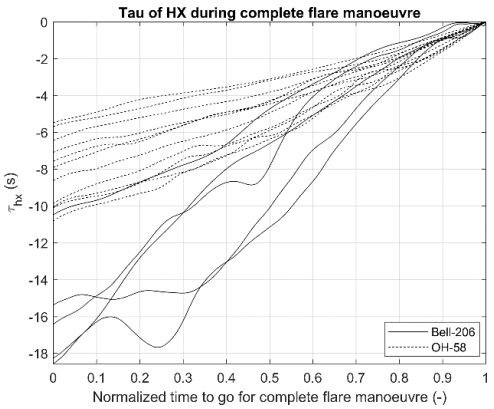

Fig. 6. Range distance, velocity and τ_{hx} during the flare manouvre.

Presented at 44th European Rotorcraft Forum, Delft, The Netherlands, 19-20 September, 2018

The method adopted to derive the extent to which the guide is followed involves performing a least-squares fit to τ_{hx} to $\tau_{g_{CDG}}$. The resulting coupling value of k is then used to make the fit. The mean R^2 values of the linear regression of the τ_{hx} and $\tau_{g_{CDG}}$ were all greater than 0.9 (see Table 1 and Table 2 in the Appendix B). Thus the data indicate a strong correlation $\tau_{hx} - \tau_{g_{CDG}}$.

Pitch angle gap close, τ_θ

The tau of pitch angle analysis was carried out in piecewise manner due to the zero-crossing of the pitch rate (q) when the maximum pitch angle is achieved during nose-up motion (Fig. 4(g)). The tau of pitch angle was analysed in two stages; first, the pitch up gap closure and second, the pitch down gap closure. The change in τ_θ is shown in Fig. 7 and Fig. 8. In the figures below, 0 in the x axis indicates the start of the gap closure manoeuvre and 1 indicates the end of the closure manoeuvre.

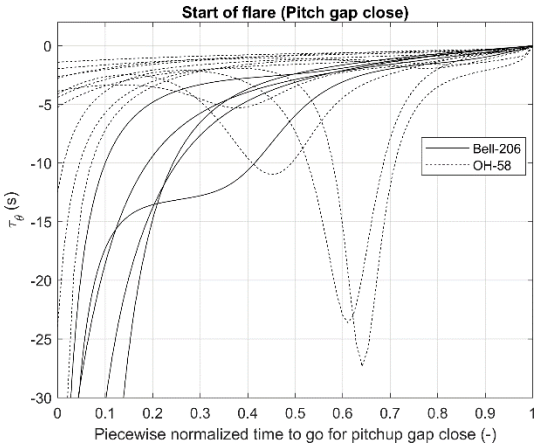

Fig. 7. Piecewise pitch angle gap τ_θ during pitchup phase of the flare manoeuvre.

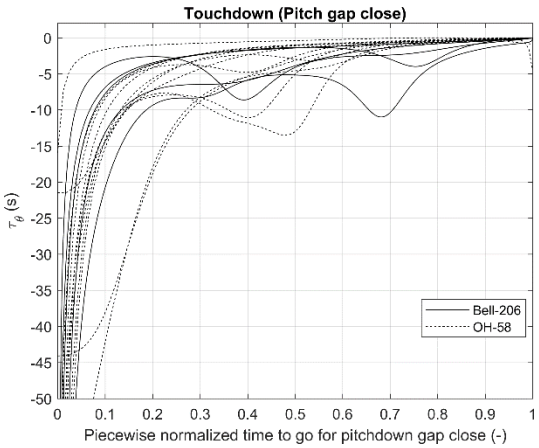

Fig. 8. Piecewise pitch angle gap τ_θ during pitchdown phase of the flare manoeuvre.

It can been seen from Fig. 7 and Fig. 8 that the form of the τ_θ motion closely resembles the constant acceleration guide (CAG) as presented in Fig. 3. The results of the classical least-square-error optimization to calculate the coupling values k is presented in Table 3 and Table 4. The values of the coupling constant, k are below 0.5. This means that the manoeuvre starts with an abrupt acceleration and the maximum pitch rate occurs towards the end of the manoeuvre. For the cases where $k = 0.4$, the maximum pitch rate occurs approximately at the mid-point, in time, through the manoeuvre. It can be noticed from the Table 3 and 4 that, for a few cases, the R^2 values are lower than 0.7. This is due to the somewhat oscillatory τ_θ responses that can be seen in Fig. 7 and Fig. 8. This is interpreted as the pilot having to stabilize the motion while closing the pitch angle gap. These extra stabilisation efforts by the pilots could be indicative of an increase in the pilot work-load in the cockpit. The "textbook" like manoeuvres suggest that this element of the manoeuvre can be modelled as a coupling between $\tau_\theta - \tau_{g_{CAG}}$.

The results presented above will be used to develop a series of algorithms that will cue the pilot to make the correct control inputs required to perform a successful and safe autorotation landing. Automated versions of the algorithms will also be assessed. However, the method outlined above and in previous work rely on the closure of a defined motion gap. This, in turn, presumes that the landing point is known. A parallel stream of work has therefore concentrated on the calculation of reachable landing locations from flare initiation. In this way, a landing location (or set of landing locations) can be selected from the determined (in real-time) reachable set on which the cueing algorithms can operate.

3. DETERMINATION OF REACHABLE LANDING LOCATIONS

The approach taken by Rogers et al[3] and in the current work is to separate the autorotation control problem into two distinct segments—a steady state descent followed by a flare to touchdown. During each of the segments, the control law must manage the aircraft's energy and orientation to ensure a safe touchdown condition and also take into account the helicopter's position such that a suitable landing location is reached. The problem of path planning in steady-state descent has received fairly substantial treatment in the literature, and an attractive planning algorithm is presented in Yomchinda *et al*[7]. However, it is likely that as the pilot approaches the flare phase of the manoeuvre, he or she is presented with better resolution of the landing area and could benefit from a visualization of the reachable landing locations. As a result, the current work focuses on

Presented at 44th European Rotorcraft Forum, Delft, The Netherlands, 19-20 September, 2018

determining the set of landing points that is reachable after the flare has been initiated. This work assumes that all heading adjustments have been accomplished during the descent phase, such that no more lateral movement is required to get to a suitable landing point (i.e., the pilot is in a final descent and will avoid turning during the flare manoeuvre).

The current work applies a low-order helicopter dynamic model developed by Carlson & Zhao et al[20] to evaluate landing trajectories generated by the landing point tracking algorithm described by Rogers *et al*[3] for an array of candidate landing points in front of the aircraft. This dynamic model has been used in various optimal control trajectory generation schemes such as the ones presented in Ref 8. However, in this work, the model is deployed in a non-iterative, real-time constraint evaluation scheme to determine feasibility of a generated landing trajectory.

Consider the complete autorotation trajectory generation and control scheme depicted in Fig. 9. This methodology integrates the controller of Sunberg et al[2], which tracks a forward speed trajectory (u_{com}) provided by the tau-based trajectory generator described in Rogers et al[3]. A key consideration of the trajectory generator scheme in Ref. 3 is that, in order to enforce runtime guarantees, no reachability criteria is enforced and thus no guarantees are provided regarding the helicopter's ability to fly such a trajectory from its current energy state. Thus, a reachability module (dashed box in Fig. 9) is developed in this paper to evaluate whether a trajectory generated by the tau-based scheme is in fact feasible from the current vehicle state.
The reachability scheme functions by generating trajectories to an array of candidate landing points in front of the aircraft. By evaluating these trajectories using a low-order model, the set of reachable points from the current helicopter state can be determined and continually updated throughout the manoeuvre. This reachability map will ultimately be cued to a pilot via a HUD for rapid reachability determination.

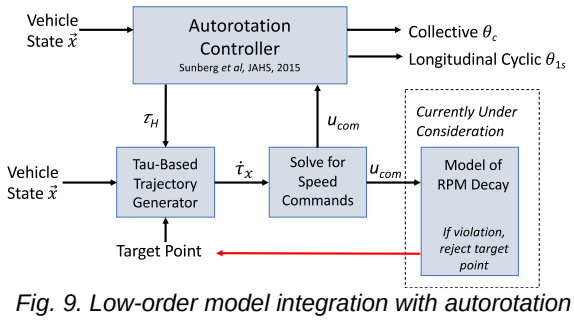

Fig. 9. Low-order model integration with autorotation controller and trajectory generator.

Note that in this approach, reachability is formulated as a constraint satisfaction problem rather than an optimal control problem. Although the predicted feasible trajectories will not be mathematically optimal, their feasibility can be guaranteed in a rapid fashion using the low-order model scheme outlined below. Moreover, this predicted reachability set is likely to be conservative through performance-limiting assumptions to the rotor speed model and its inputs.

3.1. Reduced-Order Vehicle Dynamics

The full equations of the point mass model of the helicopter in autorotation are given in Refs. 8, 10, and 20, but the primary equations are summarized here:

(8) $$m\dot{w} = mg - \rho(\pi R^2)(\Omega R)^2 C_z - \frac{1}{2}\rho f_e w\sqrt{u^2+w^2}$$

(9) $$m\dot{u} = \rho(\pi R^2)(\Omega R)^2 C_x - \frac{1}{2}\rho f_e u\sqrt{u^2+w^2}$$

(10) $$I_R\Omega\dot{\Omega} = P_s - \frac{1}{\eta}\rho(\pi R^2)(\Omega R)^3 C_P$$

(11) $$C_P = \frac{1}{8}\sigma c_{d0} + C_T\lambda$$

(12) $$C_x = C_T\sin(\alpha)$$

(13) $$C_y = C_T\cos(\alpha)$$

Note that this model captures the dynamics of the aircraft as point mass, while allowing the rotor speed dynamics to be computed using a simplified inflow model. In previous work employing this autorotation model, the dynamic equations in (8) - (10) are integrated forward in time to derive a predicted aircraft trajectory. In the current work, the model is actually solved backwards such that, given a vertical and forward deceleration profile (time histories of $\dot{u}$ and $\dot{w}$), pitch angle and rotor speed trajectories can be derived.

The output from the trajectory generating algorithm of Rogers et al[3] is an analytical forward speed profile (i.e., an analytical function of u over time) given by,

(14) $$u(t) = u_i\left(1 - \frac{(k_o-1)u_i t}{x_i}\right)^{-1-\frac{1}{k_o-1}}$$

where k_o is a constant selected to target a given desired landing site, and the i subscript represents the value of the variable at the time of trajectory generation. This profile can tracked by a pilot or an inner-loop velocity-tracking controller during the flare (see Ref 2). This function for u is differentiated to give an analytical function for the forward acceleration $\dot{u}$:

Presented at 44th European Rotorcraft Forum, Delft, The Netherlands, 19-20 September, 2018

(15) $$\dot{u}(t) = \frac{k_o u_i^2 x_i \left(1 - \frac{(k_{o-1})tu_i}{x_i}\right)^{\frac{1}{1-k_o}}}{(t(u_i - k_o u_i) + x_i)^2}$$

Given this functional form of the translational deceleration, and the vertical speed profile derived as discussed in the subsequent paragraph, Eq. (9) can be solved for the horizontal component of thrust (C_x) needed as a function of time during the flare.

A similar process is employed to derive the required vertical component of thrust C_z. This is generated by assuming a constant deceleration in the vertical direction and numerically integrating it to yield a linear vertical speed profile. The initial vertical speed is given by the helicopter state at the instant of trajectory evaluation, and the constant deceleration is selected such that the vertical speed at the final time of the trajectory is zero. This assumption allows Eq. (8) to be solved for the needed vertical component of thrust C_z as a function of time.

Given values for C_x and C_z, Eqs. (12) and (13) are then used to solve for C_T and the tip path plane angle α, which is assumed to be equal in magnitude and opposite in sign to the helicopter pitch angle. Eq. (11) is used to calculate the coefficient of power C_P. The simplified inflow equations are omitted here for brevity, but can be found in Refs. 8,10, and 20. Note that the mean profile drag coefficient of the rotor blades c_{d0} is used as a tuning parameter to match low-order model performance to a higher-fidelity model. It is assumed that there is no residual power in the shaft by the time a flare trajectory is initiated, so the shaft power P_s in (10) is set to zero. Lastly, Eq. (10) is numerically integrated forward in time from the current rotor speed using a fourth order Runge-Kutta method to yield the predicted rotor speed profile that will result from flying the input flare trajectory.

To quantify the accuracy of this model with respect to predictions from more complex models, the low-order model results are compared against results generated from a high-fidelity 6DOF helicopter model of the AH-1G Cobra[2] flying a nominal flare trajectory. To generate this data, the 6DOF model is commanded to follow a given flare trajectory using the control law in Ref. 2. The rotor speed and vehicle pitch angles from the low-order model are then compared to the actual resulting trajectory from the 6DOF. Fig. 10 shows the commanded forward speed and acceleration for the trajectory overlaid with the resulting trajectory from the 6DOF simulation. Note that the trajectory is tracked reasonably well by the inner loop controller. The other necessary input to the low-order vehicle model is an approximate vertical speed and vertical deceleration profile. These are shown in Fig. 11. Although the profiles do not match perfectly, the mismatch between assumed and desired vertical speed dynamics does not have a significant effect on model performance, as will be subsequently seen.

The outputs from the point mass model are predictions of the rotor speed and the helicopter pitch angle time histories required to fly the input flare trajectory. Examples of these outputs are shown in Fig. 12, where the results from the point mass are compared with the results of the 6DOF model. The pitch angle prediction is very close to that for the full dynamics model, except for the final two seconds, in which large decelerations are commanded by the input trajectory. The controller is unable to track these large decelerations in the 6DOF simulation because the pitch saturation limits are quite restrictive prior to touchdown. The predicted rotor speed matches the rotor speed from the 6DOF quite well as shown in Fig. 12, with an RMS error of 6% of the nominal rotor speed. Additional validation cases not shown here demonstrated that, for flare trajectories in which the rotor RPM decays below a threshold acceptable limit, the point mass rotor speed prediction decays more rapidly than the actual 6DOF model. As a result, in the majority of cases, the reachability bounds predicted by the minimum rotor speed estimates are still conservative. Additional validation cases demonstrating the accuracy and conservative nature of the point mass model predictions will be provided in follow-on work.

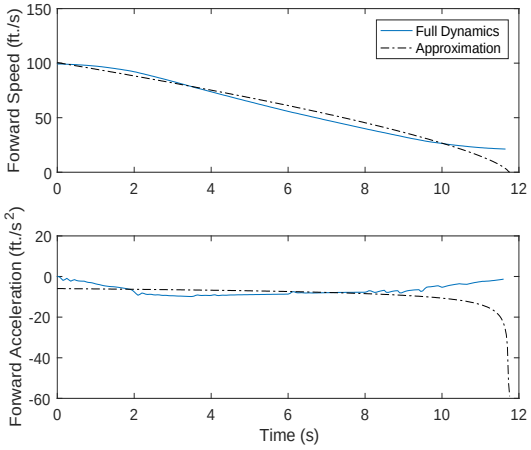

Fig. 10. . Low-order model forward channel input approximations overlaid with full AH-1G dynamic model results.

Presented at 44th European Rotorcraft Forum, Delft, The Netherlands, 19-20 September, 2018

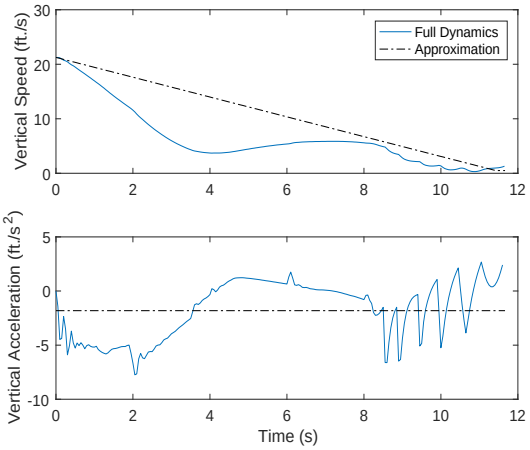

Fig. 11. Low-order model vertical channel input approximations overlaid with full AH-1G dynamic results.

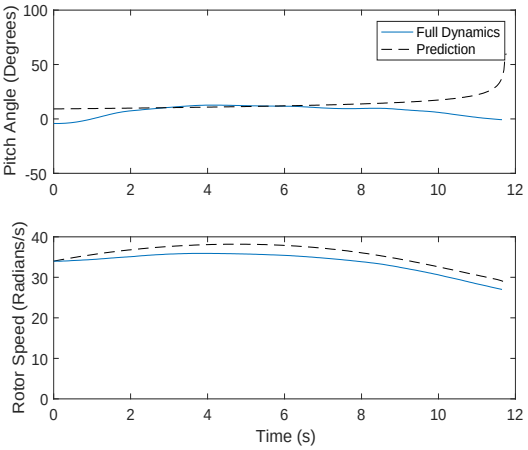

Fig. 12. Low-order model prediction overlaid with full dynamic results.

3.2. Reachable Set Determination

The set of physically reachable points is determined by generating forward speed trajectories to an array of possible target landing points in front of the aircraft, and then computing pitch angle and rotor speed predictions for each one using the process described above. These pitch angle and rotor speed trajectories are then compared against acceptable limits to determine if a trajectory is feasible. In particular, for each trajectory, the ground speed at touchdown, maximum predicted pitch angle, and maximum and minimum predicted rotor speeds are extracted from the trajectory and point mass prediction data. Because the calculations are simple and fast, the set of reachable points can be updated continually after flare initiation. An example set of predictions for the AH1-G is shown in Fig. 13. This predicted set is generated at the moment of flare entry, which makes the initial conditions for each evaluated trajectory the same. The trends in predicted values match the trends from the landing point tracking trade study conducted in Rogers et al in Ref 3. The farther the target point from flare entry, the higher the ground speed at touchdown will be. This is because the trajectory will maintain forward speed for longer, and the vehicle will not flare (pitch up) as much as it would for a closer target point where it needs to slow down more quickly. Similarly, the maximum pitch angles required to fly to points closer to the point of flare entry are higher than those needed to fly to farther points. With higher pitch angles comes increased inflow into the rotor disk, causing the autorotating rotor to spin faster. Thus, the maximum rotor speed required to fly a trajectory increases as the target point moves closer to the point of flare entry. Lastly, the minimum rotor speed is seen to decay rapidly as the candidate landing point moves beyond where the helicopter can travel. This is to be expected because the helicopter has a limited amount of total energy available at flare entry, so there is a sharp boundary beyond which rotor energy will be exhausted by the work required to decelerate the aircraft. A conservative set of reachable points is determined by enforcing upper and lower limits on each of the four states in Fig. 14, and taking the lowest upper bound and the highest lower bound over all states. This reachable set is shown at flare initiation in Fig. 14, where both the model predictions (blue dots) are shown along with the threshold lower and upper limits. Fig. 14 also includes updated reachability predictions, recomputed at 2 sec intervals as the 6DOF model flies the flare trajectory targeting a landing distance of 670 ft. beyond the point of flare entry. As expected, the set of reachable points converges on the desired landing point as the manoeuvre progresses because points that are initially reachable are no longer reachable after a certain trajectory has been flown for a period of time.

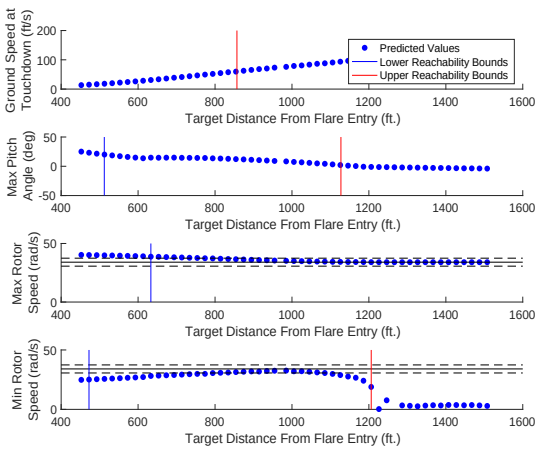

Fig. 13. Predictions of reachability metrics with example bounds overlaid.

Presented at 44th European Rotorcraft Forum, Delft, The Netherlands, 19-20 September, 2018

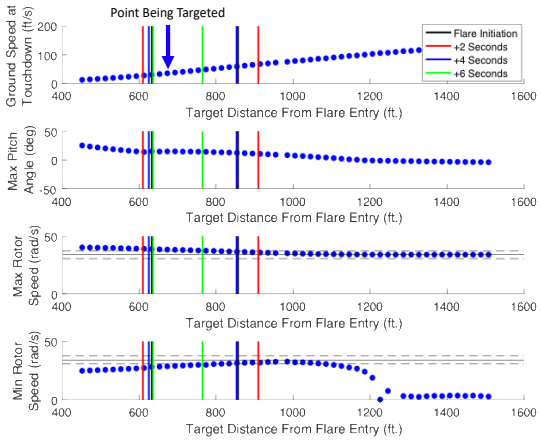

Fig. 14. Reachability boundary updates as manoeuvre progresses overlaid with initial Metric Predictions.

4. CONCLUSIONS

Tau analysis on the pitch angle gap closure and range distance gap closure during the flare phase of the autorotation manoeuvre have been performed using data from real flight tests. The analysis shows that the pitch angle motion gap closure can be modelled using the constant acceleration intrinsic motion guide (CAG) and range distance gap closure can be modelled by the constant deceleration intrinsic motion guide (CDG). Intrinsic τ-based motion guides will therefore be used to develop autorotation controllers in the future. In a related study, a scheme for computing the reachable set of landing points in autorotative flare has been proposed using a tau-based trajectory generation scheme. This reachable set computation scheme sacrifices optimality for guaranteed runtime. Preliminary results show that the trajectory generation and reachable set scheme may provide continuously-updating reachability information to a pilot as part of a cueing system for autorotation.

ACKNOWLEDGEMENT

The research/investigation was sponsored by the Army Research Laboratory and was accomplished under Cooperative Agreement Number **W911NF-16-2-0027** and the U.S. Army/Navy/NASA Vertical Lift Research Center of Excellence with Mahendra Bhagwat serving as the Program Manager and Technical Agent, grant number **W911W6-11-2-0010** and **W911W6-17-2-0002.** The views and conclusions contained in this document are those of the authors and should not be interpreted as representing the official policies, either expressed or implied, of the Army Research Laboratory or the U.S. Government. The U.S. Government is authorized to reproduce and distribute reprints for Government purposes notwithstanding any copyright notation herein. We would like to thank the National Research Council (NRC) Canada and the U.S. Naval Test Pilot's School for providing the flight test data used in this paper.

References

1 Rogers, J., Strickland, L., Repola, C., Jump, M., Cameron, N., and Fell, T., "Handling qualities assessment of a pilot cueing system for autorotation maneuvers," *Annual Forum Proceedings - AHS International*, 2017.

2 Sunberg, Z. N., Miller, N. R., and Rogers, J. D., "A Real-Time Expert Control System For Helicopter Autorotation," *Journal of the American Helicopter Society*, vol. 60, 2015, pp. 1–15.

3 Rogers, J., Eberle, B., Jump, M., and Cameron, N., "Time-to-Contact-Based Control Laws for Flare Trajectory Generation and Landing Point Tracking in Autorotation," *AHS International's 74th Annual Forum and Technology Display*, AHS International, 2018, pp. 1–12.

4 Lee, A. Y., Bryson, A. E., and Hindson, W. S., "Optimal landing of a helicopter in autorotation," *Journal of Guidance, Control, and Dynamics*, vol. 11, 1988, pp. 7–12.

5 Abbeel, P., Coates, A., Hunter, T., and Ng, A. Y., "Autonomous Autorotation of an RC Helicopter," *Springer Tracts in Advanced Robotics*, 2009, pp. 385–394.

6 Dalamagkidis, K., Valavanis, K. P., and Piegl, L. A., "Autonomous autorotation of unmanned rotorcraft using nonlinear model predictive control," *Journal of Intelligent and Robotic Systems: Theory and Applications*, vol. 57, 2010, pp. 351–369.

7 Yomchinda, T., Horn, J., and Langelaan, J., "Flight Path Planning for Descent-phase Helicopter Autorotation," *AIAA Guidance, Navigation, and Control Conference*, Reston, Virigina: American Institute of Aeronautics and Astronautics, 2011.

8 Tierney, S., and Langelaan, J. W., "Autorotation Path Planning Using Backwards Reachable Set and Optimal Control," *AHS International's 66th Annual Forum and Technology Display*, AHS International, 2010, pp. 1–13.

9 Keller, J. D., Jr, R. M. M., Horn, J. F., and Yomchinda, T., "Active Flight Control and Appliqué Inceptor Concepts for Autorotation Performance Enhancement," *American Helicopter Society Forum*, 2011.

10 "Autorotation flight control system," , January 13, 2006.

11 "Method, system, and computer program product for tactile cueing flight control," , May 6, 2003.

Presented at 44th European Rotorcraft Forum, Delft, The Netherlands, 19-20 September, 2018

[12] Jump, M., and Padfield, G. D., "Investigation of the Flare Maneuver Using Optical Tau," *Journal of Guidance, Control, and Dynamics*, vol. 29, 2006, pp. 1189–1200.
[13] Lee, D. N., "Guiding Movement by Coupling Taus," *Ecological Psychology*, vol. 10, Sep. 1998, pp. 221–250.
[14] Padfield, G. D., "The tau of flight control," *Aeronautical Journal*, vol. 115, 2011, pp. 521–556.
[15] Padfield, G. D., Lee, D. N., and Bradley, R., "How Do Helicopter Pilots Know When to Stop, Turn or Pull Up? (Developing Guidelines for Vision Aids)," *Journal of the American Helicopter Society*, vol. 48, 2003, p. 108.
[16] Lee, D. N., Craig, C. M., and Grealy, M. A., "Sensory and intrinsic coordination of movement," *Proceedings of the Royal Society B: Biological Sciences*, vol. 266, 1999, pp. 2029–2035.
[17] Lee, D. N., Davies, M. N. O., Green, P. R., and Van Der Weel, F. R., "Visual control of velocity of approach by pigeons when landing," *Closing the Gap: The Scientific Writings of David N. Lee*, 2012, pp. 106–131.
[18] Lu, L., and Jump, M., "Multiloop Pilot Model for Boundary-Triggered Pilot-Induced Oscillation Investigations," *Journal of Guidance, Control, and Dynamics*, vol. 37, 2014, pp. 1863–1879.
[19] Coyle, S., *Cyclic and collective : further art and science of flying helicopters*, Eagle Eye Solutions, 2009.
[20] Carlson, E. B., and Zhao, Y. J., "Prediction of Tiltrotor Height-Velocity Diagrams Using Optimal Control Theory," *Journal of Aircraft*, 2003, pp. 896–905.

Appendix A

Motions following a constant deceleration guide:

i. Motions begin with an abrupt deceleration which gradually eases off as the gap is closed. The larger the coupling k, the more the profile approaches the limiting case of constant deceleration ($k = 1$). In practice the initial deceleration will take a finite time to build up as will the reduction of $\dot{\tau}$ to the selected constant value.
ii. Following the guide results in $\dot{\tau_x} = k/2$ and, in theory, values of $k > 1$ are possible but result in infinite deceleration at the stop, which in practice means a collision will occur e.g. the $k = 1 \cdot 2$ case shown to illustrate such a hard-stop case.
iii. At the time the deceleration is initiated ($t = 0$), the overall time required to stop $T = -2\tau x(0)/k$; e.g. if $k = 1 \cdot 0$, then the manoeuvre time will be double the perceived τ_x at $t = 0$·

Motions following a constant acceleration guide:

i. Motions begin with an abrupt acceleration, which then subsides, with maximum velocity occurring further into the manoeuvre as k is increased. When $k = 0 \cdot 4$, the maximum velocity occurs mid-way, in time, through the manoeuvre.
ii. When $k = 0 \cdot 5$, there is a finite deceleration at the end of the manoeuvre; when $k > 0 \cdot 5$, an infinite deceleration is required to close the gap, which, in practice, means a collision will occur.
iii. As the manoeuvre comes to a close $t \rightarrow 1$, $\widehat{\tau'} \rightarrow k$, asymptotic to the constant deceleration guided motion, noting that k (constant acceleration) is actually half of k (constant deceleration).

Appendix B

Table 1.Coupling of τ_{hx} with constant intrinsic deceleration guide in flare phase during autorotation for OH-58 type helicopter.

No. of run	1	2	3	4	5	6	7	8	9	10	11
k, coupling	0.92	0.87	0.90	0.94	0.90	0.96	0.90	0.91	0.96	0.85	0.82
R^2 – linear regression	0.96	0.92	0.95	0.98	0.98	0.93	0.94	0.97	0.92	0.91	0.86

Table 2.Coupling of τ_{hx} with constant intrinsic deceleration guide in flare phase during autorotation for Bell-206 type helicopter.

No. of run	1	2	3	4	5
k, coupling	0.64	0.65	0.60	0.68	0.72
R^2 – linear regression	0.98	0.97	0.98	0.96	0.94

Presented at 44th European Rotorcraft Forum, Delft, The Netherlands, 19-20 September, 2018

Table 3. Coupling of τ_θ with constant intrinsic acceleration motion guide in flare phase during autorotation for OH-58 type helicopter.

No. of run	**1**	**2**	**3**	**4**	**5**	**6**	**7**	**8**	**9**	**10**	**11**
k, pitchup	0.40	0.47	0.36	0.45	0.36	0.33	0.48	0.29	0.45	0.28	0.30
R^2 – linear regression	0.67	0.79	0.69	0.74	0.70	0.79	0.87	0.65	0.78	0.72	0.91
k, pitchdown	0.42	0.44	0.40	0.49	0.27	0.35	0.45	0.32	0.42	0.30	0.32
R^2 – linear regression	0.90	0.86	0.94	0.90	0.91	0.81	0.49	0.68	0.98	0.86	0.99

Table 4. Coupling of τ_θ with constant intrinsic acceleration motion guide in flare phase during autorotation for Bell-206 type helicopter.

No. of run	**1**	**2**	**3**	**4**	**5**
k, pitchup	0.36	0.31	0.42	0.40	0.42
R^2 – linear regression	0.80	0.99	0.97	0.95	0.91
k, pitchdown	0.35	0.33	0.43	0.42	0.40
R^2 – linear regression	0.96	0.84	0.97	0.93	0.77

Presented at 44th European Rotorcraft Forum, Delft, The Netherlands, 19-20 September, 2018